Structure of sleep explained by wave mechanics.

Vasili Kharchenko[1,2] and Irina V. Zhdanova[3,4]

Author information:
1. Department of Physics, University of Connecticut, Storrs, Connecticut 06269, USA.
2. Institute for Theoretical Atomic, Molecular & Optical Physics, Harvard-Smithsonian Center for Astrophysics, Cambridge MA 02138, USA
3. Department of Anatomy and Neurobiology, Boston University School of Medicine, Boston, MA 02118, USA.
4. BioChron LLC, Worcester, Massachusetts 01605, USA (current address)

Keywords: sleep dynamics, NREM, REM, wave mechanics, probability waves, coherent superposition, sleep cycle invariant

The physiological state of sleep is crucial for maintaining overall health and well-being, yet its function and dynamics remain largely unexplained. Humans experience two distinct types of sleep, non-rapid eye movement (NREMS) and rapid eye movement (REMS), which alternate and change in duration and intensity over multiple sleep cycles. Understanding this complex sleep architecture, especially since REMS manifests a paradoxical mix of sleep and wake features, is a key challenge in the field. Here we show that, by adapting the formalism of wave mechanics, human sleep dynamics can be modeled as an interaction between probability waves representing Sleep and Wake states, with REMS corresponding to their coherent superposition. The wave model provides an accurate quantitative description of the changes in duration and intensity of NREMS and REMS episodes during regular and extended sleep, and correctly predicts their specific responses to sleep deprivation and abundance. The functional unity between NREMS and REMS proposed by the model predicts the existence of a sleep cycle invariant, the product of NREMS duration and REMS intensity, that remains constant across consecutive cycles of undisturbed sleep. Overall, the wave model of sleep dynamics presents a comprehensive framework and an advanced mathematical tool for studying both normal sleep and sleep disorders.

Regular alternations between the two main physiological and behavioral states, Wake and Sleep, are a classical example of dynamic homeostasis[1]. Complex biological systems, such as the human body, are characterized by numerous interacting feedback loops and their spatial and temporal coherency, which help to maintain dynamic stability within physiological limits[2,3]. Wake-related activities lead to internal changes that increase the instability of intrinsic processes and disrupt their coherency, together increasing Wake state instability[4-7]. This manifests as increasingly unstable neurobehavioral performance and occurrence of involuntary microsleeps that compromise adaptive responses. To prevent potentially harmful consequences, spontaneous transitions from metastable Wake to Sleep state are normally initiated before the physiological limits are reached.

Despite extensive knowledge of the neuronal mechanisms that control sleep[8], our understanding of the biological substrate of sleep homeostasis and its dynamics is limited[9]. Human sleep has a complex structure known as sleep architecture, which typically includes five to six sleep cycles per night (Fig. 1a). Each sleep cycle consists of two types of Sleep: non-rapid eye movement sleep (NREMS), followed by rapid eye movement sleep (REMS). In contrast to Wake state, both NREMS and REMS are characterized by low perception of the environment, but they are otherwise remarkably different states of the organism. Gradual disengagement from the environment in NREMS is associated with slowing of brain activity and reduced muscle tone, though ability for motor activity is preserved. Paradoxically, REMS manifests as high brain activity and rapid eye movements, active dream mentation, irregular heart rate and respiration, and sexual arousal, all on the background of further reduction of perception, loss of muscle tone and thermoregulation[10,11]. This unique combination of wake-like and sleep-like features makes the nature and significance of REMS particularly puzzling.

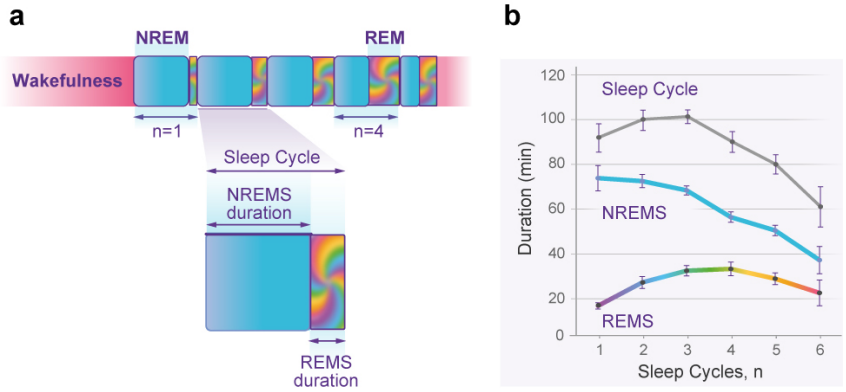

Fig. 1 Human sleep architecture.
a. Schematics of consolidated sleep pattern, consisting of consecutive sleep cycles, each including longer NREMS (cyan) and shorter REMS (multicolor) episodes. Five sleep cycles are shown, n.
b. Typical changes in the duration (min) of consecutive sleep cycles (black), NREMS (cyan) and REMS (multicolor) episodes over regular nighttime sleep. Mean±SEM, 24 young healthy volunteers, 39 sleep nights total (Method 16).

Understanding the complex patterns of sleep dynamics involving quasi-periodic oscillations between the two types of sleep is a key challenge in the field. The stochastic nature of dynamic sleep process, which is sensitive to internal and external perturbations, results in inter-individual and night-to-night variation in sleep architecture. However, on average, overnight sleep patterns show typical gradual changes in the duration and intensity of NREMS and REMS episodes (Fig. 1b). Previous phenomenological and mathematical models have tested a range of theoretical approaches[12-15] to sleep architecture, including simple homeostatic relationship between NREMS and REMS[16], the postulation of a specialized REMS oscillator that is active only during sleep[17], and ultradian oscillations generated by homeostatic and circadian forces[1,18] based on classical mechanics[13]. While these models describe qualitatively realistic patterns of sleep-like oscillations, they have not been able to quantitatively reproduce the typical sleep architecture (Fig. 1b). These models also do not reconcile some important qualitative features of sleep dynamics, such as (*i*) the opposing changes in NREMS and REMS, with the initial prolonged high-intensity NREMS and short low-intensity REMS, and the later shorter low-intensity NREMS and longer high-intensity REMS; (*ii*) the duration of consecutive REMS episodes first increasing and then declining, in contrast to REMS intensity showing linear increase, or (*iii*) NREMS intensity dropping mid-sleep, much faster than the gradual decline in the duration of NREMS episodes.

We chose to look at sleep dynamics through the prism of wave mechanics, which describes the coherent, spatiotemporal behavior of multiple interacting oscillators that form waves. In biological systems, where coherent behavior of homeostatic feedback loops is essential, the wave processes are common, providing rapid spatiotemporal coordination and preservation of signal amplitude[19]. While comparing the dynamics of Sleep and Wake states to other wave processes, we found notable similarities with the dynamics of probability waves in quantum physics, specifically in diatomic molecule[20]. As detailed in Methods, the similarities include the probabilistic nature of both Sleep and Wake states and molecular states, the quasi-periodic sleep cycles resembling cycles of molecular vibrations, and the mixed Sleep-Wake state (rapid eye movement sleep) reminiscent of a coherent superposition of distinct molecular states that can form the quantum-mechanical entanglement[20, 21]. Although the suggested Sleep and Wake waves are clearly not of quantum mechanical nature, it is well established that the stochastic classical systems can mimic the dynamics of probability waves observed in quantum physics[22-26]. Together, this motivated us to use the mathematical apparatus of quantum mechanics to describe sleep dynamics. Here we show that the probability wave concept and mathematical apparatus of wave mechanics can provide an accurate quantitative description of typical human sleep architecture.

The wave model of Sleep dynamics.

The overall concept of our wave model of sleep dynamics is illustrated in Figure 2. The probability of being in Sleep or Wake state is modeled by two interacting waves, shaped by the corresponding Morse potential wells U_S and U_W (Fig. 2a; Extended Fig. 1; Method 1-3). The waves propagate along the regulating parameter of state stability x – a one-dimensional reduction of the overall physiological state. It reflects the collective action of

various parameters of the system and regulates coherent behavior of the underlying processes. Per usual wave mechanics treatment, the two interacting waves, whose joint probability density is normalized to unity, describe the probability of observing an individual in any point of the regulating parameter space (Method 1). Low values of x favor the Wake state, while high values favor the Sleep state.

Normally, during daytime wakefulness, the aggregate action of homeostatic, circadian, and environmental forces gradually drives the system to higher values of x, moving it further away from the parametric region of stable Wake state (Fig. 2a,b). The rise in Wake state instability is formally described as increase in the model parameter ε or, in analogy to physical systems, the energy of state instability accumulated due to the work of the driving forces (Fig. 2a,b). During this process, the unstable homeostatic Sleep-Wake equilibrium is reached around the x_c-point, the crossing of $U_S(x)$ and $U_W(x)$ potential curves (Fig. 2a). This corresponds to the homeostatic energy threshold $U(x_c)$ (Fig. 2b), around which the distance between the two potential curves is minimal, increasing an interaction between the two states and probability of Wake→Sleep transition. However, in humans, the daytime driving forces of circadian[18] and environmental nature effectively inhibit Sleep-Wake interaction and state transition, prolonging consolidated Wake state, increasing x further and raising ε beyond $U(x_c)$. For simplicity, our model allows the driving force to gradually increase the energy along the U_W wall, since the cyclic structure of the Wake state is not fully understood and is not the focus of the current model.

At night, the driving forces subside, and relaxation of the accumulated energy can then move the system back to the original state of stable wakefulness. However, the relaxation of x and ε (Fig. 2b) occurs only during Sleep state and involves a stepwise process. Spontaneous Wake→Sleep state transition (sleep onset) occurs at x_o at the initial U_S level j_{in}, generating a sleep wavepacket with energy $\varepsilon_{j_{in}}$ (Fig. 2a; Method 4, 5). This initiates the series of sleep cycles, with each cycle resulting in a transition to a lower energy level (Fig. 2a; Method 4).

During NREMS part of the sleep cycle, the wavepacket oscillates between the walls of U_S and, through time-evolution, a portion of its energy is prepared for release. This is analogous to the transformation of the wavepacket of unstable (excited) molecular or atomic electronic state in preparation for emitting excessive energy. The decline in the period of x oscillations defines the decrease in the duration of consecutive NREMS episodes, while ε_j and decline in x amplitude define rapid drop in NREMS intensity[27] (Fig. 2b; Extended Fig. 1; Methods 5, 13).

Towards the end of each cycle, when the wavepacket approaches U_W, i.e., the Wake state, it releases a discrete portion of energy $\Delta\varepsilon$, equal to the energy gap between neighboring levels. This occurs within the x_c region of Sleep-Wake equilibrium, where the interaction between the Sleep and Wake waves is increased (Fig. 2a,c; Methods 6-9). The interaction results in a delay of the wavepacket propagation and incorporation of Sleep and Wake waves, forming their coherent superposition[20] that in our model corresponds to REMS (Fig. 2c). The duration of REMS episode of each cycle is determined by the lifetime τ of the coherent superposition at the corresponding energy level. This lifetime depends on the strength of Sleep-Wake interaction that peaks at the crossing of the two potentials at $U(x_c)$ and is strong enough to create a resonant state (Methods 8-10) with a distinct resonance level j_c (Fig. 2c).

Consistent with the Lorentz resonance curve, the closer the energy of the wavepacket is to the energy of j_c level, the longer the τ and the duration of REMS (Fig. 2d). This relationship defines the bell-shaped curve of consecutive REMS durations (Fig. 1a; Methods 11,12). Thus, the model predicts that that the higher the initial energy level reached over prolonged wakefulness, the larger the difference between j_{in} and j_c, and the smaller the duration of REMS episode due to weak resonance. The model also predicts that REMS intensity correlates with the magnitude of $\Delta\varepsilon$ released at the end of each sleep cycle (Fig. 2a,c). The changes in this experimental measure would then follow a linear increase in energy gaps of the Morse potential (Fig. 2a,d).

Over consecutive sleep cycles, the stepwise release of the energy of state instability brings the system closer to relatively stable Wake state. Accordingly, the longer the Sleep-Wake coherent superposition (REMS duration) or the more energy of state instability is lost (REMS intensity), the higher the probability of Sleep →Wake transition, explaining why spontaneous awakening positively correlates with longer or more intense REMS[28,29]. Both the probability of Sleep↔Wake transition (i.e., sleep or wake propensity) and REMS duration are strongly affected by the circadian clock[18] due to time-dependent modulation of the strength of the Sleep-Wake interaction (Method 1). This study focuses on normal sleep under regular entrained conditions, with stable adaptive synergy of circadian and homeostatic regulation. The model predictions on specific contribution of circadian and homeostatic regulation to Sleep-Wake interaction are to be detailed in a separate report.

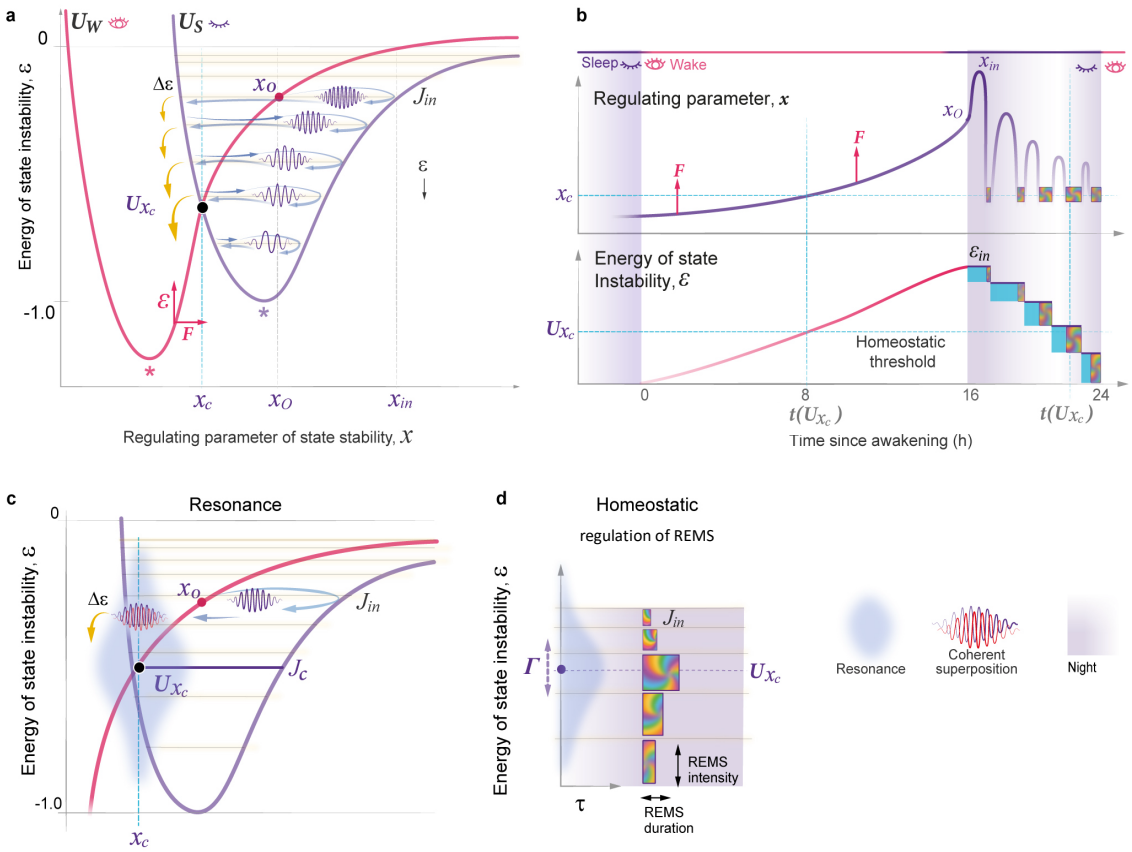

Fig. 2 The schematics of the wave model of Sleep dynamics.

a. In the Wake state (U_W, red potential), the driving force F (horizontal red arrow) increases the regulating parameter x (x-axis) beyond the Sleep-Wake homeostatic equilibrium x_c (vertical cyan line), rising the energy of state instability ε (vertical red arrow and y-axis) above the homeostatic energy threshold (Ux_c, black dot; the crossing point of the two potential curves). Sleep state (U_S, purple potential) starts at x_o (sleep onset, red dot) of the initial energy level j_{in} (first sleep cycle). Relaxation of x and ε occurs in the form of sleep wavepacket propagating along energy levels (blue arrows), where x_{in} – maximal deviation. At the end of each cycle, around x_c, a portion of the wavepacket energy $\Delta\varepsilon$ (yellow arrows) is released. Stars– maximal stability of the corresponding state. The schematics serves to only illustrate the concept. For actual position of Ux_c and j_{in} within U_S see Extended figure 2.

b. *Top panel:* Time-dependent changes in the regulating parameter of state stability x (y-axis) over Wake (white area) and Sleep (purple area). In Sleep, the period of x oscillations corresponds to the duration of consecutive NREMS episodes, while decline in their amplitude squared to the drop in NREMS intensity. Each cycle ends around x_c (horizontal cyan line), the region of Sleep-Wake equilibrium where REMS episodes occur (multicolor blocks). F – the driving force (red arrow) that increases x.

Bottom panel: Time-dependent changes in the energy of state instability ε (y-axis) over the Wake state (white area) and during stepwise decline over consecutive sleep cycles (block width - duration: NREMS – cyan; REMS - multicolor). Maximal energy level reached (ε_{in}) defines initial NREMS intensity. The linearly increasing portions of energy released $\Delta\varepsilon$

correspond to REMS intensity (block height). Horizontal cyan line - potential energy of homeostatic threshold, $U(x_c)$. Vertical cyan line – timing of $U(x_c)$, with daytime timing arbitrary placed mid-day; x-axis – time since awakening (hours).

c. Around the crossing point $U(x_c)$ of U_S (purple potential) and U_W (red line), strong Sleep-Wake interaction creates the resonance level j_c and resonance state (gray area) with energy-dependent (ε) strength (width of gray area). The propagation of the sleep-wavepacket (purple) is temporarily delayed by the resonance within the x_c region. The wavepacket then incorporates the Sleep and Wake waves and forms their coherent superposition (red-purple wavepacket). This represents REMS, allowing for the release of a portion of energy $\Delta\varepsilon$ (yellow arrow). For actual typical position of j_c see Extended fig. 2.

d. The resonance strength (width of gray area) and resonance width Γ (vertical double arrow) define the lifetime of coherent superposition τ (x-axis) at each energy level and thus REMS episode duration of each sleep cycle. REMS duration (multicolor block width) peaks around the resonance level and the homeostatic threshold $U(x_c)$ (black dot), and declines at lower levels. Unlike that, REMS intensity (multicolor block height) increases linearly, as per the energy gaps of the Morse potential, $\Delta\varepsilon$ (yellow arrow).

Quantitative modeling of experimentally observed human sleep architecture.

The wave model predicts that it takes only two model parameters (Fig. 3a), the width of the potential well and the number of the energy level at which Sleep state is initiated, to describe the dynamics of NREMS episode duration and intensity, and REMS episode intensity (Method 12-14). Describing the REMS episode duration requires two additional parameters of the Sleep-Wake resonance, its width and energy level (Fig. 3a; Methods 11,12).

First, we tested the model's ability to quantitatively describe the dynamics of experimentally observed NREMS and REMS episode durations. We focused on average episode durations in groups of individuals with normal sleep (Method 16), as individual sleep patterns exhibit stochastic behavior that would require additional considerations, such as probabilistic treatment of model parameters and the effects of intrinsic and environmental noise. To do this, we analyzed data on regular sleep, collected from our 24 young, healthy volunteers for a total of 39 nights of 9-h sleep opportunity. We also analyzed a dataset on extended sleep promoted by four weeks of exposure to 14-h sleep-favoring conditions, as collected by Barbato and Wehr[30] from 11 young, healthy individuals over a total of 308 nights.

Figures 3b and 3c demonstrate that the model exhibits remarkable quantitative agreement with both regular and extended sleep data sets (χ^2 goodness of fit test P>0.88 and P>0.99, respectively), accurately capturing the monotonic decrease of NREMS durations and the bell-shaped curve of REMS durations. The duration of the first NREMS episode was excluded from the statistical assessment of fit since, as the model predicts, it was curtailed by approximately a quarter of that predicted for the initial energy level (Fig. 3b,c). This is because the position of the sleep onset x_o occurs somewhere between the two potential walls (Fig. 2a). Consistent with the model prediction that habitual sleep duration positively correlates with the width of U_S potential, it was increased by 13% in the extended sleep group (Extended Table 1).

We then addressed quantitative description of the intensities of both types of sleep. Conventionally, NREMS intensity is evaluated based on the power of slow-wave activity (SWA) in the brain cortex or the duration of slow-wave sleep (SWS)[27]. It is enhanced following prolonged wakefulness and displays a rapid initial decline during Sleep. The model predicts that the initial NREMS intensity and the rate of its decline positively correlate with the maximal energy reached at the initial level, $\varepsilon_{j_{in}}$. The model also predicts that the rate of decline in NREMS intensity over consecutive sleep cycles is proportional to the square of the x amplitude (Fig. 2b). This is consistent with the general rule that the intensity of a wave is proportional to the square of its amplitude L^2. Therefore, NREMS intensity can be expressed as κL^2, where the coefficient κ is inversely proportional to $|\varepsilon|$, the absolute value of wavepacket energy (Method 13). Note that, in general, ε values in a potential well are presented as negative (Fig. 2a,c), so an increase in ε leads to a lower $|\varepsilon|$.

To test our prediction regarding NREMS intensity, we compared the SWS durations in the experimental groups with regular and extended sleep to our model's predictions, which were based on the parameters obtained from

the analysis of their NREMS episode durations (Fig. 3b,c; Extended Table 1). Within each group, NREMS intensity was normalized to the first sleep cycle. We found that our theoretical curves are in good agreement with experimentally observed dynamics of NREMS intensity for both groups (Fig. 2e, χ^2 P>0.99 for both datasets). The rapid decline of L^2 in the Morse potential, which outpaces the decline in ε, can explain why NREMS intensity flattens out mid-sleep, before the energy of state instability is sufficiently reduced for spontaneous awakening.

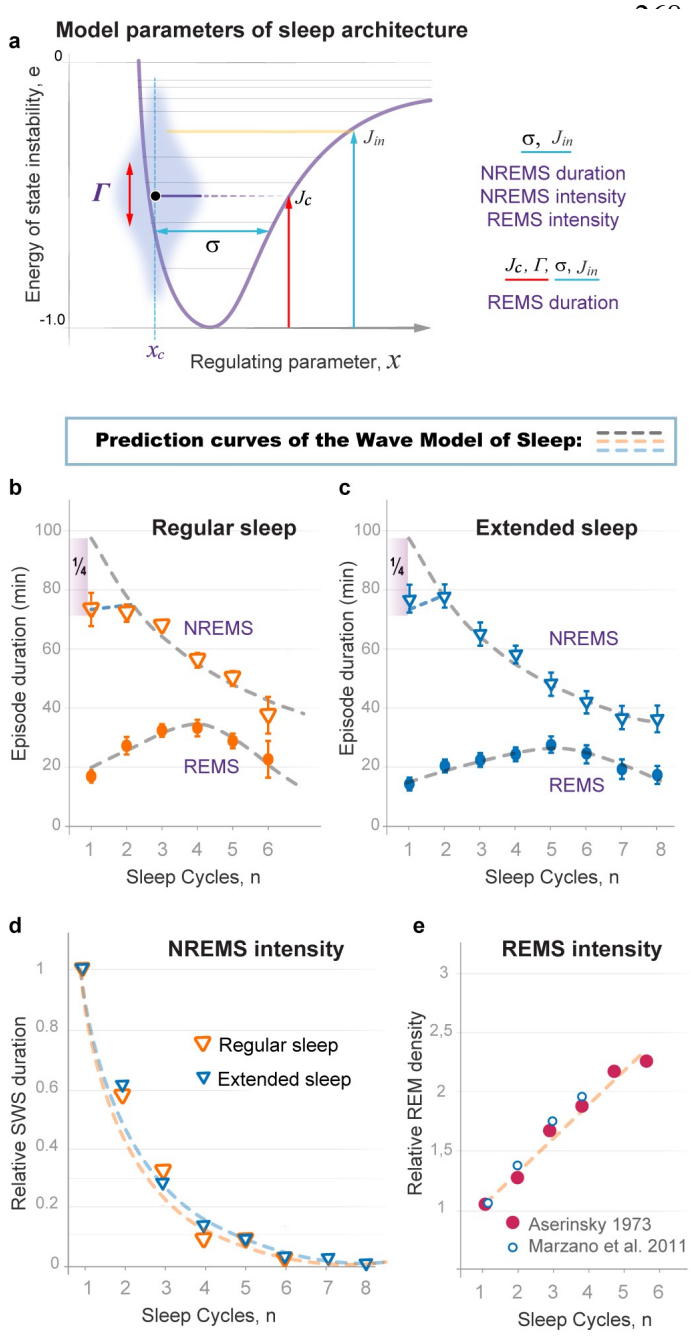

Figure 3 The wave model of sleep provides accurate quantitative description of normal sleep architecture.
a. Four model parameters are predicting sleep architecture: σ– width of U_S potential (cyan double-arrow); J_{in} – energy level at sleep initiation (yellow line); J_c – resonance energy level (dashed line); Γ- resonance width (red double-arrow). Cyan arrows –two parameters defining NREMS episode duration and intensity, and REMS episode intensity. Red arrows – two additional parameters predicting REMS episode duration. Gray - resonance region. Black dot - homeostatic threshold $U(x_c)$.
b. Episode durations over regular sleep: Theoretical curves (dashed lines) and experimental data (mean ±SEM) for NREMS (triangle) and REMS (circle) episode durations (min), as a function of the sleep cycle order number n (x-axis). Due to J_{in} being populated at a variable point x_o (see Fig. 2a), the first experimental NREMS episode duration is, on average, ¼-th shorter than the theoretical one for this energy level. Data collected in 24 young healthy subjects, 39 nine-hour nights (Method 16). R^2 values: NREMS: 0.905; REMS: 0.811.
c. Episode durations over extended sleep: Theoretical curves (dashed lines) and experimental data (mean ±SEM) for NREMS (triangle) and REMS (circle) episode durations (min), as a function of the sleep cycle order number n (x-axis). Data collected in 11 young healthy subjects, 308 fourteen-hour nights, as reported by Barbato & Wher[30]. Shorter first NREMS episode duration is explained in b. R^2 values: NREMS: 0.993; REMS: 0.965.
d. Theoretical curves (dashed lines) and experimental data (triangles) for the decline in NREMS intensity over consecutive sleep cycles (*n*; x-axis) of regular sleep (shown in b., orange) and extended sleep (shown in c.; Barbato et al.[29], blue). Mean group data for Slow Wave Sleep duration is normalized to the first sleep cycle. R^2 values: Regular sleep: 0.973; Extended sleep: 0.990.
e. The rate of linear increase in REMS intensity (REM density) over consecutive sleep cycles is similar in independent groups of young healthy subjects with regular sleep. Experimental data collected by Aserinsky[28] (red circle) and Marzano et al.[33] (open circle) relative to theoretical data (dashed line) of the wave model based on the increase in energy gaps Δε predicted for a similar experimental group (shown in b.). Mean group data for REM density is normalized to the first sleep cycle. R^2 values: Aserinsky: 0.961; Marzano: 0.997.

Conventionally, REMS intensity is evaluated based on the number of eye movements per minute of REMS episode (REM density)[32]. Our model predicts that REMS intensity in each sleep cycle is proportional to the amount of energy $\Delta\varepsilon$ released during transition to a lower energy level, which occurs in REMS. Since energy gaps in the Morse potential are small at high energy levels and increase linearly as the energy is relaxed (Fig. 2a), the model predicts that REMS intensity should also be small at the sleep start and increase linearly over

consecutive REMS episodes (Fig. 3e). The experimental data accumulated over the past decades fully supports these model predictions[28, 32-34].

Strong validation of our model was provided by comparing the theoretical and experimental slopes of linear increase in REMS intensity over regular sleep period. In the model, the slope is defined by two parameters, the number of the energy level at sleep initiation, which depends on the duration of prior wakefulness, and the width of the potential well, which depends on habitual sleep duration (Fig. 3a; Extended Table 1; Method 14). The model thus suggests that groups with similar sleep durations prior to and over the experimental period should have similar REMS intensity slopes. To test this, we compared the regular sleep REM density data collected in groups of young healthy volunteers by Aserinsky[28] and Marzano et al.[33]. Figure 3d illustrates that the slope angles are almost identical between these independent experimental groups and match well the slope predicted by the model for our similar experimental group with regular sleep (Method 16; χ^2 P >0.99 for both datasets). The latter theoretical slope is based exclusively on the documented NREMS episode durations for regular sleep (Fig. 3b), without any additional adjustment of parameters.

The model predicts that the duration of prior wakefulness has specific effects on the initial measures of normal sleep architecture. Longer Wake state leads to higher initial energy $\varepsilon_{j_{in}}$, smaller energy gaps $\Delta\varepsilon$ between top levels and larger difference between j_{in} and j_c (Fig. 2a-c). As a result, following sleep deprivation, sleep starts with higher NREMS intensity, lower REMS intensity and shorter REMS episode duration, respectively. In contrast, when sleep onset follows prior sleep abundance and shorter wakefulness, it is associated with lower $\varepsilon_{j_{in}}$, larger $\Delta\varepsilon$ and smaller difference between j_{in} and j_c. This predicts lower NREMS intensity, higher REMS intensity and longer REMS episode duration of the first sleep cycle, respectively. Due to variable point x_o of sleep onset (Fig. 2a) and occurrence of "skipped REMS" following sleep deprivation (τ is too short to be reliably documented), first NREMS episode duration is a less predictable parameter. These qualitative model predictions are in full agreement with extensive experimental data on the effects of sleep deprivation and sleep abundance [7,27,28-33].

Prediction of the Sleep Cycle Invariant.

Figure 4 illustrates that, within each cycle, the duration of the NREMS episode corresponds to the period of oscillation of the Sleep wavepacket along x-axis, which is inversely proportional to the energy gap between levels, $1/\Delta\varepsilon$. The intensity of the REMS episode is directly proportional to the energy released at the end of this cycle, $\Delta\varepsilon$. This allows us to predict that, under ideal circumstances, the product of the NREMS episode duration and the intensity of the subsequent REMS episode should yield a constant value over consecutive cycles of normal sleep (Method 5, 14, 15). We refer to this parameter as the Sleep Cycle Invariant (SCI). Intrinsic stochasticity of the Sleep state, internal and external interferences, or circadian phase shift may alter the stability of SCI, and validation of this prediction requires datasets with high statistical power for both NREMS duration and REMS intensity documented in parallel.

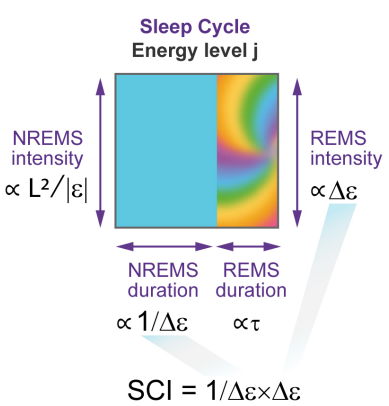

Figure 4. Sleep cycle as a structural and functional unit of sleep.
Experimental sleep parameters (purple font) are proportional to model parameters (black font). NREMS duration is ∝ to the period of x oscillation and thus inverse ∝ to the energy gap, $1/\Delta\varepsilon$. NREMS intensity is ∝ to $L^2/|\varepsilon|$, where L is the amplitude of x oscillation and $|\varepsilon|$ is the absolute value of wavepacket energy. REMS duration is ∝ to τ, the lifetime of coherent superposition. REMS intensity is ∝ to energy gap, $\Delta\varepsilon$. The sleep cycle invariant (SCI), being the product of NREMS duration and REMS intensity, ideally should remain constant over consecutive sleep cycles. Cyan – NREMS, multicolor -REMS.

Discussion/Conclusions

The present study found that a model of Sleep and Wake states as interacting probability waves accurately describes typical human sleep architecture, including the durations and intensities of non-rapid eye movement sleep (NREMS) and rapid eye movement sleep (REMS) episodes. The model also made accurate qualitative predictions about the effects of sleep deprivation and sleep abundance on sleep architecture. Although the model may appear complex, it produces simple analytical formulas that can be used to efficiently analyze large datasets.

The wave model proposes that the conventional structural unit of sleep, the sleep cycle (Fig. 1, 4), is also a basic functional unit, with the sequence in which the two types of sleep occur within the cycle reflecting their distinct functions. The model suggests that NREMS gradually prepares the system for the release of a portion of the energy of state instability, moving the system into a configuration of coherent superposition of Sleep and Wake states. This coherent superposition of the two waves corresponds to REMS and allows for energy release. This is consistent with REMS manifesting a paradoxical combination of Sleep and Wake features[11]. In remarkable analogy to quantum physics where the coherent superposition can form a novel entangled state[21], the notion of REMS being a distinct "third state" of consciousness is supported by strong experimental evidence[35].

The model's accurate quantitative description of the experimentally observed durations and intensities of NREMS and REMS episodes validates this overall concept. The documented REMS intensity being directly proportional to the energy of instability lost within each sleep cycle is in line with the original proposition by Eugene Aserinsky, the discoverer of REMS[10], that REMS intensity provides a measure of "sleep satiety"[32]. The concept is also reflected in the fundamental prediction of the Sleep Cycle Invariant (SCI) that unites NREMS duration and REMS intensity. The SCI should ideally remain constant over consecutive sleep cycles of normal sleep, and its variation due to intrinsic and extrinsic interferences may provide a novel measure of sleep quality.

It takes just two model parameters, the width of the potential well and energy reached over prior wakefulness (Fig. 3a), to accurately predict the duration of NREMS episodes and intensities of both NREMS and REMS, in spite of their distinctly different overnight dynamics. The model suggests that these two model parameters are normally defined by habitual sleep duration and time awake prior to sleep initiation, respectively. This is supported by accurate quantitative prediction of sleep parameters for the extended sleep (Fig. 3c,d) being associated with increase in the width of the potential and qualitative predictions for the documented effects of sleep deprivation or abundance. The analysis of sleep architecture in naturally short- and long-sleepers could provide further validation of the model.

The homeostatic relationship between the Sleep and Wake states is undisputed. However, previous models have not formalized the homeostatic threshold, relying mostly on the limits provided by the circadian clock[1]. In contrast, the wave model of sleep dynamics includes a critical homeostatic energy threshold that reflects the point of equilibrium and strong interaction between the Sleep and Wake states, and is associated with a higher probability of prolonged REMS duration. As a result, the time when the sleep process is near the homeostatic threshold can be estimated based on the peak of the REMS duration curve. Individual differences in this threshold are likely to be significant for understanding variations in normal sleep and sleep disorders.

The model operates with the Sleep and Wake probability waves not of quantum mechanical nature. However, the stochastic classical systems are known to mimic the dynamics of probability waves observed in quantum physics[22-26] and we consider our finding to be yet another example of this phenomenon. We propose that the conceptual and mathematical apparatus of wave mechanics can be applied to the study of multiple aspects of both Wake and Sleep states, including changes induced by acute and chronic sleep deprivation, circadian phase shifts, disease, pharmacological or environmental interventions.

Bibliography

1. Borbély, AA, Achermann, P. Sleep homeostasis and models of sleep regulation. *J Biol Rhythms.* 1999 Dec;**14**(6):557-68. doi: 10.1177/074873099129000894. PMID: 10643753.
2. Ashby, W. R. (1960). *Design for a Brain: the Origin of Adaptive Behaviour*. Chapman: London, 2nd edition.
3. Kelso, J. A. S. (1995). *Dynamic Patterns: the Self-organization of Brain and Behavior*. MIT Press.
4. Doran, SM, Van Dongen, HPA, Dinges DF. Sustained attention performance during sleep deprivation: evidence of state instability. *Arch Ital Biol.* 2001; **139**(3):253–267.
5. Goel, N, Rao H, Durmer, JS, Dinges DF. Neurocognitive consequences of sleep deprivation. *Semin Neurol*. 2009 Sep;**29**(4):320-39. doi: 10.1055/s-0029-1237117.
6. Zhou, X; Ferguson, SA; Matthews, RW; Sargent, C; Darwent D; Kennaway DJ; Roach GD. Dynamics of neurobehavioral performance variability under forced desynchrony: evidence of state instability. *Sleep* 2011;**34**(1):57-63.
7. Cajochen, C., Khalsa S.B.S., Wyatt, J.K., Czeisler, C.A., and Dijk D.J. 1999. EEG and ocular correlates of circadian melatonin phase and human performance decrements during sleep loss. *Am. J. Physiol.* **277**: R640.
8. Scammell, TE, Arrigoni, E, Lipton JO. Neural Circuitry of Wakefulness and Sleep. *Neuron.* 2017 Feb 22;**93**(4):747-765. doi: 10.1016/j.neuron.2017.01.014. PMID: 28231463; PMCID: PMC5325713.
9. Krueger, JM, Frank, MG, Wisor, JP, Roy S. Sleep function: Toward elucidating an enigma. *Sleep Med Rev.* 2016 Aug;**28**:46-54. doi: 10.1016/j.smrv.2015.08.005.
10. Aserinsky, E and Kleitman, N. Regularly occurring periods of eye motility, and concomitant phenomena, during sleep. *Science.* 1953 Sep 4;**118**(3062):273-4. doi: 10.1126/science.118.3062.273. PMID: 13089671.
11. Peever, J, Fuller PM. The Biology of REM Sleep. *Curr Biol.* 2017 Nov 20;**27**(22):R1237-R1248. doi: 10.1016/j.cub.2017.10.026. PMID: 29161567.
12. Achermann, P, Borbély, AA. Mathematical models of sleep regulation. *Front Biosci.* 2003 May 1;**8**:s683-93. doi: 10.2741/1064.
13. Phillips, AJ, Robinson, PA, Klerman EB. Arousal state feedback as a potential physiological generator of the ultradian REM/NREM sleep cycle. *J Theor Biol.* 2013 Feb 21;**319**:75-87. doi: 10.1016/j.jtbi.2012.11.029.
14. Le Bon, O. Relationships between REM and NREM in the NREM-REM sleep cycle: a review on competing concepts. *Sleep Med.* 2020 Jun;**70**:6-16. doi: 10.1016/j.sleep.2020.02.004.
15. Heller, HC. Question what is "known". *Neurobiol Sleep Circadian Rhythms.* 2021 Feb 24;**10**:100062. doi: 10.1016/j.nbscr.2021.100062. PMID: 33681534; PMCID: PMC7930578.
16. Benington, JH, Heller, HC. Does the function of REM sleep concern non-REM sleep or waking? *Prog Neurobiol.* 1994 Dec;**44**(5):433-49. doi: 10.1016/0301-0082(94)90005-1. PMID: 7886233.
17. Massaquoi, S. G. & R. W. McCarley: Extension of the limit cycle reciprocal interaction model of REM cycle control. An integrated sleep control model. *J Sleep Res* **1**, 138-143 (1992)
18. Czeisler, CA, Gooley, JJ. Sleep and circadian rhythms in humans. *Cold Spring Harb Symp Quant Biol.* 2007;**72**:579-97. doi: 10.1101/sqb.2007.72.064. PMID: 18419318.
19. Deneke, VE, Di Talia, S. Chemical waves in cell and developmental biology. *J Cell Biol.* 2018 Apr 2;**217**(4):1193-1204. doi: 10.1083/jcb.201701158.
20. Landau. LD. and Lifshitz, EM, *Quantum Mechanics*. *Non-relativistic Theory*. Pergamon Press, 1977, ISBN: 9780080209401 eBook ISBN: 9781483149127
21. Wineland. D.J., Nobel Lecture: Superposition, entanglement, and raising Schrödinger's cat. 2013 *Rev. Mod. Phys.* **85**, 1103
22. Bush, J., and Oza, A., Hydrodynamic quantum analogs, 2020, *Rep. Prog. Phys.* **84**, 017001 (41pp)

23. Couder, Y. and Fort, E., Single-Particle Diffraction and Interference at a Macroscopic Scale, Phys.Rev.Lett., 2006, 97, 154101, doi: 10.1103/*PhysRevLett*.**97**.154101
24. Eddi, A., Moukhtar, J., Perrard, S., Fort, E., and Couder, Y., Level Splitting at Macroscopic Scale, Phys.Rev.Lett., 2012,108, 264503, doi: 10.1103/*PhysRevLett.***108**.264503
25. Vandewalle, N., Bouncing droplets mimic spin systems, *Nature*., Vol **596**, 5 August 2021 ,p. 41
26. Perrard ,S., Labousse, M., Miskin, M., Fort, E., and Couder, Y., Self-organization into quantized eigenstates of a classical wave-driven particle, 2014, *Nature Communications* |,**5**:3219 | doi: 10.1038/ncomms4219, doi: 10.1038/ncomms4219
27. Dijk, DJ. Regulation and functional correlates of slow wave sleep. J Clin Sleep Med. 2009 Apr 15;**5**(2 Suppl):S6-15. PMID: 19998869; PMCID: PMC2824213.
28. Aserinsky, E. Relationship of rapid eye movement density to the prior accumulation of sleep and wakefulness. *Psychophysiology.* 1973 Nov;10(6):545-58. doi: 10.1111/j.1469-8986.1973.tb00804.x. PMID: 4356207.
29. Barbato, G, Barker, C, Bender, C, Giesen, HA, Wehr, TA. Extended sleep in humans in 14 hour nights (LD 10:14): relationship between REM density and spontaneous awakening. *Electroencephalogr Clin Neurophysiol.* 1994 Apr;**90**(4):291-7. doi: 10.1016/0013-4694(94)90147-3. PMID: 7512910
30. Barbato, G. and Wehr, TA., 1998, Homeostatic regulation of REM sleep in humans during extended sleep. *SLEEP*, 1;**21**(3):267-76. doi: 10.1093/sleep/21.3.267.
31. Dijk DJ, Brunner DP, Borbély AA. Time course of EEG power density during long sleep in humans. *Am J Physiol.* 1990 Mar;**258**(3 Pt 2):R650-61. doi: 10.1152/ajpregu.1990.258.3.R650.
32. Aserinsky, E. The maximal capacity for sleep: rapid eye movement density as an index of sleep satiety. *Biol Psychiatry.* 1969 Apr;**1**(2):147-59. PMID: 4312855.
33. Marzano, C, De Simoni, E, Tempesta, D, Ferrara, M, De Gennaro, L. Sleep deprivation suppresses the increase of rapid eye movement density across sleep cycles. *J Sleep Res.* 2011 Sep;**20**(3):386-94. doi: 10.1111/j.1365-2869.2010.00886.x. Epub 2010 Sep 5. PMID: 20819146.
34. Khalsa, SB, Conroy, DA, Duffy, JF, Czeisler, CA, Dijk, DJ. Sleep- and circadian-dependent modulation of REM density. *J Sleep Res.* 2002 Mar;**11**(1):53-9. doi: 10.1046/j.1365-2869.2002.00276.x. PMID: 11869427.
35. Chow, HM, Horovitz, SG, Carr, WS, Picchioni, D, Coddington, N, Fukunaga, M, Xu, Y, Balkin, TJ, Duyn, JH, Braun, AR. Rhythmic alternating patterns of brain activity distinguish rapid eye movement sleep from other states of consciousness. *Proc Natl Acad Sci U S A.* 2013 Jun 18;**110**(25):10300-5. doi: 10.1073/pnas.1217691110. PMID: 23733938.

METHODS

In this section, we first outline the analogies between the Sleep-Wake dynamics and the model of a diatomic molecule that informed our work (**a-f**). Next, in Methods **1-15**, we detail the wave model of normal human sleep dynamics and explain how the comparisons between the experimental data and theoretical predictions were made. Method **16** describes the experimental datasets (our and others) that were used to validate the model and includes the Inclusion and Ethics statement for our dataset. Method **17** details the statistical testing.

It is important to note that human sleep is a stochastic process, as reflected in the high inter-individual and night-to-night variation of sleep architecture. Therefore, this work is intended to model average sleep patterns in groups of human subjects studied under well-controlled conditions. Additionally, it should be noted that the wave model in this paper only addresses normal human sleep.

We view the dynamics of the Sleep state as the result of the interaction of two probability waves formed by numerous coherent biochemical oscillators that require coherence. In developing the mathematical approach, we

drew a structural analogy with a quantum mechanics model of a diatomic molecule[20] and relied on several key parallels:

a) **Fast and slow components determine the dynamics of the system.** In a diatomic molecule, changes in electronic states are fast, while changes in the distance between the nuclei of the two atoms (the internuclear distance R) are slow. In our model, changes in biochemical and electrochemical processes forming Sleep or Wake state are relatively fast, while changes in the regulating parameter of state stability x are slow and thus analogous to variations in R.

b) **State stability of the fast component.** In the molecular system, the electron component can be in stable (ground) or unstable (excited) state, which are states of different symmetry at a given value of R. Changes in R can result in the swap of symmetry of the state, such that a former ground state becomes unstable, while the former excited state becomes stable. Similarly, in our model, the stability of the Sleep and Wake states is determined by the regulating parameter x, and changes depending on variations in x value. Low x values favor Wake and high x values favor Sleep

c) **The interaction and feedback relationship between the fast and slow components.** For different electronic states in a diatomic molecule, the energy of the fast (electronic) component depends on R, and this dependence creates a potential energy U(R) for the slow nuclear motion. We expect a similar relationship within the Sleep and Wake dynamics, where the parameter x regulates the stability of the underlying fast processes, e.g., homeostatic loops. In turn, those fast processes modulate the dynamics of the regulating parameter x, creating distinct potential energies $U_S(x)$ and $U_W(x)$, respectively.

d) **Probability waves.** The wave nature of probabilistic processes can be illustrated by the probability waves, or de Broglie waves, which describe the dynamics of the electronic and nuclear components in a diatomic molecule. The non-deterministic nature of the Sleep and Wake processes, as well as the coherent dynamics of their slow and fast components, suggests the use of quantum mechanical analogies in the description of Sleep architecture.

e) **State transitions.** The probabilistic transitions between electronic states of different symmetry, that is the swapping of stable and metastable (excited) states, can occur within certain restricted regions of the R-parameter where the electronic energies of different states have close values. We predict that transitions between the Sleep and Wake states will have similar behavior in the region of crossing or pseudo-crossing of the $U_S(x)$ and $U_W(x)$ potential curves. The x_c represents the point of Sleep-Wake homeostatic equilibrium, with Ux_c as the homeostatic energy threshold (Fig. 2a).

f) **The discrete energy spectra of the stationary probability waves.** In the molecular system, the stationary probability waves have a discrete spectrum of energy for both the electronic and nuclear components, the latter being represented by R-vibrations. In analogy, in our model we introduce the energy parameter ε that represents the measure of instability for either Wake or Sleep state. Increase in state instability leads to increase in ε.

Wave model of Sleep-Wake dynamics

1. **Wave equations for the Sleep and Wake states.** It has been demonstrated through both experimental and theoretical studies that classical systems can mimic behaviors commonly associated with quantum mechanics, such as energy level quantization, tunneling, spin structures, and double-slit interference, among others. These effects have been observed in some macroscopic systems containing classical stochastic waves near instability threshold[22-26]. We thus suggested that the probability waves for Sleep (S) and Wake (W) can be also described using a mathematical analogy with probability waves in

quantum mechanics. This enabled the use of the two-component Schrödinger equation for the slow nuclear motion in diatomic molecule to describe the motion of the regulating parameter *x* in our model.

The amplitudes and phases of S and W probability waves are described by the time-dependent wave functions $\Psi_S(x,t) * |s,x>$ and $\Psi_W(x,t) * |w,x>$, where $|s,x>$ and $|w,x>$ are the wave functions of the fast intrinsic variables of underlying S and W processes, which are regulated by the *x* variable. These functions, which are analogues of the wave functions of different electronic states in a diatomic molecule, are orthogonal at any *x* and *x'* because of $<x,s|w,x'> = 0$. The functions $\Psi_S(x,t)$ and $\Psi_W(x,t)$ describe the dynamics of the variable *x* in both S and W states and two-component wave equations can be written in the matrix form:

$$i\frac{\partial}{\partial t}\begin{pmatrix}\Psi_S(x,t)\\ \Psi_W(x,t)\end{pmatrix} = \begin{pmatrix}\widehat{H}_{SS}(x) & V_{S,W}(x,t)\\ V_{W,S}(x,t) & \widehat{H}_{WW}(x)\end{pmatrix}\begin{pmatrix}\Psi_S(x,t)\\ \Psi_W(x,t)\end{pmatrix} + \widehat{D}\,(x,t)\begin{pmatrix}\Psi_S(x,t)\\ \Psi_W(x,t)\end{pmatrix}, \qquad (1)$$

$$\widehat{H}_{SS}(x) = -\frac{1}{2}\frac{d^2}{dx^2} + U_S(x) \quad \text{and} \quad \widehat{H}_{WW}(x) = -\frac{1}{2}\frac{d^2}{dx^2} + U_w(x)\,, \qquad (2)$$

where $U_S(x)$ and $U_W(x)$ are the potential energies modulating propagation of S and W waves, respectively, and $V_{S,W}(x,t) = V^*_{W,S}(x,t)$ is the matrix element of the operator responsible for the interaction between S and W states. Note that $V_{S,W}$ reflects both the *x*-dependent and time-dependent interstate interaction, including the entrained 24-h periodicity in the Sleep-Wake cycle that is controlled by the circadian system[18]. Efficient S↔W state transitions can be induced by the S-W interaction near the crossing point of the $U_S(x)$ and $U_W(x)$ potential curves. Although the potentials U_S and U_W exist simultaneously at the same coordinate *x*, each affects only the corresponding wave. The time, coordinate, and energies in equations 1 and 2 are dimensionless values measured in their specific units. The normalization of the wave functions $\int_{-\infty}^{+\infty} dx\,(\,|\Psi_S|^2 + |\Psi_W|^2) = 1$ provides the probabilities of realization of S or W state: $P_S(t) = \int_{-\infty}^{+\infty} dx\ |\Psi_S|^2$ and $P_W(t) = \int_{-\infty}^{+\infty} dx\ |\Psi_W|^2$.

The operator $\widehat{D}\,(x,t)$ in Eq.1 includes the driving force F, which increases the energy of the system, and forces that damp the kinetic energy of the *x*-coordinate. The closest quantum analogy with Eqs.1 and 2 is the system of equations for the nuclear motion of diatomic molecules with two electronic states of different symmetry[20, 36]. In this mathematical analogy, the electronic states represent fast underlying processes regulated by the value of microscopic interatomic distance. However, in the dynamics of macroscopic probability waves[22-26], as we assume the S and W waves are, the time and spatial scales are many orders of magnitude greater than those described in quantum physics. The time-evolution of wave functions $\Psi_S(x,t)$ and $\Psi_W(x,t)$ determines the entire dynamics of S and W states, and consequently the Sleep architecture.

2. S and W stationary waves. Complete sets of eigen functions (stationary waves) can be used as a standard mathematical tool for the determination of wave functions satisfying Equations 1 and 2. The equations for S and W stationary waves can be obtained by neglecting the S-W interaction ($V_{S,W} = 0$) and the action of the $\widehat{D}\,(x,t)$ operator. In this case, the stationary S-waves $\Psi_{S,j}(x,t) = \exp(-i\,\varepsilon_j\,t) * \varphi_j(x)$ and W-waves $\Psi_{W,k}(x,t) = \exp(-i\,\varepsilon_{w,k}\,t) * \psi_k(x)$ are expressed via two sets of independent eigen functions $\varphi_j(x)$ and $\psi_k(x)$, and their eigen energies ε_j and $\varepsilon_{w,k}$, respectively. Since the objective of our model is an accurate description of the Sleep architecture, we mainly consider the stationary S-waves representing the bound states of the potential $U_S(x)$ with a discrete set of energies ε_j (*j*=0,1,2,3…). The experimental data on the architecture of the W state is limited, and the analysis of W stationary waves is beyond the scope of our model. However, the wave model suggests that the interaction of S and W states plays a key role in the energy relaxation during sleep, specifically in the process of energy release, and that this is reflected in sleep architecture.

3. Energy spectra of the S-waves in the Morse potential. The quasi-periodic nature of the sleep cycles with gradually reducing durations of NREMS episodes T_{NR} (Fig.1b) indicates that neither parabolic nor rectangular potential wells can describe the Sleep process (Extended Fig.1). In contrast, the Morse potential $U_S(x)$, commonly used in atomic and molecular physics, provides a set of energy levels ε_j that are sufficient for accurate quantitative description of the S-wave propagation and the energy relaxation process. The one-dimensional Morse potential is given by the equation:

$$U_S(x) = U_0 * \left(e^{-2\frac{x}{\sigma}} - 2e^{-\frac{x}{\sigma}}\right), \qquad (3)$$

where U_0 and σ are positive constants that describe the depth and width of the potential well, respectively. Our model is designed to predict the relative values of T_{NR} in different seep cycles, so we can scale the depth of U_S potential, $U_0 = 1$. As a result, the energies ε_j at each level and the corresponding eigen wave functions depend on the single parameter σ. The spectra of the discrete energy levels ε_j of the Morse potential are given by the following equation[20]:

$$\varepsilon_j = \varepsilon_j(\sigma) = -\left(1 - \frac{j+\frac{1}{2}}{N(\sigma)}\right)^2 \quad (j = 0,1,2, \dots j_{Max}) \qquad (4)$$

where $N(\sigma) = \sqrt{2}\sigma$ is the dimensionless parameter that regulates the the total number of discrete energy levels in the Morse potential, $j_{Max} = \left[N(\sigma) - \frac{1}{2}\right]$.

The discrete energy spectrum and wave functions of stationary waves can also be approximated using quasi-classical Bohr-Sommerfeld model[20,37]. The quasi-classical approximation illustrates the connection between wave and particle dynamics, and describes propagation of the wavepackets of probability waves. We will later consider the dynamics of the quasi-classical wavepacket of S-waves and thus determine the NREMS episode durations, T_{NR}. In the Morse potential, the period of oscillations of the wavepacket moving with an energy close to ε_j declines as the energy ε_j drops, while the energy gaps $\Delta\varepsilon(j) = \varepsilon_j - \varepsilon_{j-1}$ between consecutive levels increase (Fig. 2a; Extended Fig.1).

4. Energy relaxation and structure of the S-wavepacket. Spontaneous W→ S transition initiating Sleep generates a wavepacket of S waves with the initial energy $\varepsilon \approx \varepsilon_{j_{in}}$. Relaxation of the instability energy ε in stepwise transitions, $j \to j-1$, occurs through the release of discrete portions of energy $\Delta\varepsilon(j) = \varepsilon_j - \varepsilon_{j-1}$. The level $j(n)$ occupied by the wavepacket during the n-th sleep cycle of the relaxation process is determined by the initial level j_{in} and the order number n of the sleep cycle (Fig. 1a,b, 2a), $j(n) = j_{in} - n + 1$. In the general case, the exact composition of the wavepacket with an arbitrary energy ε includes all stationary S waves belonging to the discrete and continues spectra. At the same time, in the quasi-classical approximation, it can be mostly represented by a single S-wave from j energy level, if ε is close to the energy level ε_j. For simplicity, we neglect the wavepacket dispersion over the entire relaxation process and consider that the wavepacket energy $\varepsilon_{j(n)}$ is reduced only in the stepwise $j(n) \to j(n+1)$ transitions during REMS episodes.

5. Quasi-classical motion of the wave packet. At large j, the period T_j of quasi-classical oscillations of the center of the wavepacket corresponds to the period of motion of a classical particle with energy ε_j bouncing between the potential walls of $U_S(x)$. T_j can be expressed through the energy difference between the neighboring energy levels[37]: $T_j = 2\pi/(\frac{\partial\varepsilon_j}{\partial j}) \approx 2\pi/\Delta\varepsilon(j)$, where the derivative $\frac{\partial\varepsilon_j}{\partial j}$ has been replaced with the energy gap $\Delta\varepsilon(j)$. The wavepacket motion is also quasi-classical at lower energy levels j where the Morse

potential is similar to the potential of the harmonic oscillator (equation 3 and Fig. 2a). The unitless value of T_j is given by the equation:

$$T_j = \frac{2\pi}{\Delta\varepsilon(j)} = 2\pi \frac{1}{\varepsilon_j(\sigma) - \varepsilon_{j-1}(\sigma)} = 2\pi \frac{\sigma^2}{\sqrt{2}\,\sigma - j} \qquad (5)$$

The discrete set of T_j reflects the discrete structure of the energy spectra ε_j of S stationary waves. The set of consecutive $T_{j(n)}$ periods with $j = j(n)$ predicts the relative durations of consecutive NREMS episodes $T_{NR}(n)$, i.e., periods of the quasi-classical motion in the Morse potential. These values depend only on the width of the potential well σ and an actual level j occupied by the wavepacket during the n-th sleep cycle.

6. Interaction between S and W stationary waves and their coherent superposition. The independence of S and W states is strongly violated within the δx_c region of non-adiabatic behavior around the crossing point x_c (Fig.2a,c), where the interaction $|V_{S,W}(x,t)|$ is larger than or comparable to the difference between the potential energies: $|U_S(x) - U_W(x)| \lesssim |V_{S,W}(x,t)|$[20]. Thus, inside $\delta x_c \sim \left|V_{S,W}(x,t)\right| / \left| \frac{\partial U_S}{\partial x} - \frac{\partial U_W}{\partial x} \right|_{x=x_c}$, the stationary S and W waves can form a coherent superposition or entanglement. The formation of S-W entanglement inside the moving wavepacket can be clarified by a simplified example in which an entangled state is constructed from isolated stationary S and W waves. A two-state model includes a single S-wave eigenstate $\varphi_s(x)$ and single eigenstate of W-wave $\psi_w\,(x)$ with energies ε_s and ε_w, and a time-independent potential of S-W interaction $V_{S,W}(x,t) = V(x)$ can be used to explain this phenomenon. This interaction creates new stationary waves with new energies $E_{a,b}$ and the wave functions $\Psi_{a,b}(x,t) = \chi_{a,b}(x) * e^{-i\,E_{a,b}t}$, where new eigen functions $\chi_{a,b}(x)$ are expressed via the coherent superposition of the unperturbed $\varphi_s(x)$ and $\psi_w\,(x)$ waves of S and W states:

$$\begin{cases} \chi_a(x) = cos\frac{\theta}{2} * \varphi_s(x) + \ sin\frac{\theta}{2} * \psi_w\,(x) \quad , \\ \chi_b(x) = -\sin\frac{\theta}{2} * \varphi_s(x) + cos\frac{\theta}{2} * \psi_w\,(x) \ , \end{cases} \qquad (6)$$

The eigen energies $E_{a,b}$ and coefficients of the coherent superposition $cos\frac{\theta}{2}$ and $sin\frac{\theta}{2}$ are given by the equations:

$$E_{a,b} = \frac{\varepsilon_s + \varepsilon_w}{2} \mp \sqrt{\frac{\Delta\varepsilon_{sw}{}^2}{4} + \tilde{V}_{s,w}{}^2} \ , \ \Delta\varepsilon_{sw} = \varepsilon_s - \varepsilon_w \ , \ \text{ and } \ cos\theta = \frac{1}{\sqrt{1 + \left(2\frac{\tilde{V}_{s,w}}{\Delta\varepsilon_{sw}}\right)^2}} \quad , \qquad (7)$$

where $\tilde{V}_{SW} = \int_{-\infty}^{+\infty} dx\ \varphi_s^*(x) V(x) \psi_w(x)$ is the matrix element of the S-W interaction potential, and θ is the mixing angle. For simplicity, we assumed zero values of the diagonal matrix elements, $\tilde{V}_{SS} = \tilde{V}_{WW} = 0$. Note that the energies $E_{a,b}$ of the new states differ from the energy levels of U_S and U_W potentials. The probabilities p_s and p_w to detect the characteristic features of S and W states in the new stationary wave $\Psi_a(x,t)$ are expressed in terms of the coefficients of coherent superposition: $p_s = cos^2\frac{\theta}{2}$ and $p_w = sin^2\frac{\theta}{2}$. Under condition of weak state interaction, i.e., $\theta \ll 1$, the new stationary wave $\chi_a(x)$ is mainly represented by $\varphi_s(x)$, occupying primarily the region of S stability $x > x_c$. The second stationary wave $\chi_b(x)$ is located predominantly within the region of W stability $x < x_c$ and it is represented mostly by $\psi_w(x)$. The parameter of perturbation $\beta = \left| \frac{\tilde{V}_{s,w}}{\Delta\varepsilon_{sw}} \right|$ describes the relative strength of the interaction $\tilde{V}_{s,w}$ and regulates the fractions of W and S state within their coherent superposition, $\Psi_{a,b}(x,t)$. In case of $\beta \to 0$, i.e., weak S-W interaction or very large energy difference $\Delta\varepsilon_{sw}$, the entanglement is not formed. In contrast, large value of $\tilde{V}_{s,w}$ or small difference between S and W energy levels ($\beta \gg 1$ or $\Delta\varepsilon_{sw} \to 0$) creates conditions for strong coherent mixing of S and

W waves. In this case, the mixture angle is $\theta = \frac{\pi}{2}$, the wave mixture coefficients are $cos\frac{\theta}{2} = sin\ \frac{\theta}{2} = 1/\sqrt{2}$, and the coherent S-W superpositions $\frac{1}{\sqrt{2}}\ [\varphi_s(x) \pm\ \psi_{\ w}(x)]$ include equal fractions of S and W waves.

The condition of $\Delta\varepsilon_{sw} \rightarrow 0$ can be seen as a resonance between two stationary waves of different symmetry. Accidental resonance can occur between stationary waves contained within different potential wells[38]. Under conditions of wavepacket propagation, its motion is considered as an adiabatically slow process and the mechanism of formation of coherent states includes similar mixing of the stationary waves, with one important difference: the entanglement of the S and W states is temporary and lasts for as long as the center of the wavepacket remains inside the non-adiabatic region δx_c.

7. The coherent superposition of S and W waves and the wavepacket dynamics. In the energy relaxation process, the wavepacket is composed mainly of $\varphi_{j(n)}(x)$ waves and its center moves like a classical particle, bouncing between $U_S(x)$ walls (Fig. 2a). Within this semi-classical approximation, transitions between W and S states can occur when the center of the wavepacket approaches the δx_c region where the crossing of $U_S(x)$ and $U_W(x)$ potential curves enhances the efficiency of S and W interaction. Within δx_c, the wavepacket can temporarily incorporate a substantial fraction of stationary W waves, as shown in equations 6 and 7. The S-W interaction creates a delay τ in the wavepacket propagation, and leads to a new temporary state represented by the coherent superposition of S and W waves. Thus, an organism can simultaneously exist in both S and W states over the time interval τ, until the wavepacket leaves δx_c region. In our model, this new state corresponds to REMS, coherently incorporating S and W features. The τ defines the lifetime of the coherent superposition within δx_c and thus REMS episode duration T_{REM}.

8. Short time-delay induced in Landau-Zener transition. The presence of the region of the enhanced S-W interaction $V_{S,W}$, i.e., the region of non-adiabatic behavior of S state, leads to additional accumulation of the phase $\eta(\varepsilon)$ of the stationary wave with energy ε, and thus the delay in the wavepacket propagation. The resulting time-delay $\tau(\varepsilon)$ can be calculated using the energy dependence of the wave phase shift, $\eta(\varepsilon)$: $\tau(\varepsilon) = 2\frac{d\eta(\varepsilon)}{d\varepsilon}$ [39]. The time delay $\tau_{LZ}\ (\varepsilon)$ of the wavepacket passing through δx_c can be also estimated using the semi-classical Landau-Zener model[20]:

$$\delta x_c \sim \frac{|V_{SW}(x_c)|}{|\frac{\partial U_S}{\partial x} - \frac{\partial U_W}{\partial x}|_{x=x_c}} \qquad \text{and} \qquad \tau_{LZ}\ (\varepsilon_j) \sim \frac{\delta x_c}{v_j} = \frac{|V_{SW}(x_c)|}{v_j\ \ |\frac{\partial U_S}{\partial x} - \frac{\partial U_W}{\partial x}|_{x=x_c}}\ ,$$

where v_j is the velocity of the classical particle moving with energy ε_j through the x_c region. Usually, the Landau-Zener model cannot provide long τ because interaction potential $V_{SW}(x)$ is considered as a small perturbation with respect to $U_S(x)$ and $U_W(x)$. In our model, τ_{LZ} is the background time-delay in the absence of the resonance process. General mathematical analysis and experimental data on the non-adiabatic transitions and phase accumulation for the extended Landau-Zener model have been reported in[40-43].

9. The resonance enhancement of REMS episode duration and energy release. Within δx_c, the presence of W-wave component of the wavepacket leads to the action of the damping forces included into the operator $\widehat{D}\ (x,t)$, as shown in equation 1. This allows for the wavepacket to release a fraction of its energy $\Delta\varepsilon(j)$, corresponding to the energy gap between the *j* and *j*-1 levels. At a constant value of damping forces, the efficiency of the energy release depends on the strength of S-W interaction and the time-delay $\tau(\varepsilon_j)$. The value of the released energy $\Delta\varepsilon(j)$ increases with the number of cycles *n*. Facilitating energy release requires more time for the action of the damping forces, i.e., increasing $\tau(\varepsilon_j)$. This can be accomplished through a resonance condition for the incoming S-wave, if the energy of the resonance level ε_{jc} is close to $U(x_c)$, the potential energies of S and W states near their crossing point x_c, where the strength of S-W interaction is high. The

temporary capture of the wavepacket into the resonance state augments the lifetime of coherent S-W superposition and thus T_{REM}.

10. Mechanisms of resonance formation. The formation of a resonance state can occur through different mechanisms. One example is the Feshbach resonance[44], in which the energy levels of $U_S(x)$ and $U_W(x)$ are located near $U(x_c)$. In this case, $\tau(\varepsilon_j)$ determines the effective time that the W-state is present within the composition of the S-wavepacket when the center of the wavepacket is located within the δx_c region. Another mechanism by which an S-wave resonance may occur is through a very strong local interaction between the S and W waves, which creates a quasi-bound state localized near x_c. In this case, the avoided crossing structure of the adiabatic potentials can support the resonance (quasi-bound) state for incoming S-waves and temporarily localize the wavepacket within δx_c . Detailed mathematical descriptions of these resonance effects have been developed in the theory of slow atomic collisions[45]. For either mechanism, the energy of the S-wave resonance ε_{jc} can be formally associated with the resonance level j_c.

11. Lorentz resonance curve. Independent of the mechanism of the resonance, at any energy ε_j of the S wavepacket, the resonance time-delay $\tau(\varepsilon_j)$ is sensitive to the energy difference between ε_j and the resonance energy ε_{jc}. The time-delay can be calculated from the additional resonance phase $\eta(\varepsilon_j)$[39] with a simple expression for the resonance value of $\tau(\varepsilon_j)$ given by the resonance Lorentz formula[39,44]:

$$\tau(\varepsilon_j) = 2\frac{d\eta(\varepsilon\ )}{d\varepsilon}\Big|_{\varepsilon=\varepsilon_j} = \frac{1}{\pi}\ \frac{\frac{\Gamma}{2}}{(\varepsilon_j - \varepsilon_{jc})^2 + (\frac{\Gamma}{2})^2}\ , \qquad (8)$$

where ε_{jc} and Γ are the energy level and width of the S-wave resonance, respectively. The j_C value can be expressed via $U(x_c)$: $j_c \cong \sqrt{2}\,\sigma\left(1 - \sqrt{|U(x_c)|}\,\right) - \frac{1}{2}$. It is not an integer because, in the general case, the resonance energy does not exactly match ε_j levels. The dynamic changes of $\tau(\varepsilon_{j(n)})$ over the process of stepwise energy relaxation describe relative durations of consecutive REMS episodes $T_{REM}(n)$ over the course of sleep.

12. NREMS and REMS episode durations in absolute time units. The $T_{NR}(n)$, and $T_{REM}(n)$ in absolute time units (min) can be obtained using equations 5 and 8 for the relative durations $T_{j(n)}$ and $\tau(\varepsilon_{j(n)})$ with $j(n) = j_{in} - n + 1$, and the absolute time scaling constants A_{NR} and A_{REM}, respectively:

$$T_{NR}(n) = A_{NR}\ T_{j\{n\}} = \ A_{NR}\ 2\pi\frac{\sigma^2}{\sqrt{2}\,\sigma - j_{in} + n - 1}\ , \qquad (9)$$

$$T_{REM}(n) = \ A_{REM}\ \tau\left(\varepsilon_{J(n)}\right) = \ A_{REM}\ \frac{1}{\pi}\ \frac{\frac{\Gamma}{2}}{(\varepsilon_{j_{in}-n+1} - \varepsilon_{jc})^2 + (\frac{\Gamma}{2})^2}\ , \qquad (10)$$

To calculate the relative values of $T_{NR}(n)$, two model parameters are needed: the width of U_S potential σ and the initial level j_{in}. To calculate the relative values of $T_{REM}(n)$, two additional model parameters are required: the energy ε_{jc} of the resonance level and the resonance width Γ (Fig. 3a). These parameters have been inferred from comparisons of the experimental data on $T_{NR}(n)$ and $T_{REM}(n)$ and the theoretical predictions of these values given by the analytical formulas in equations 9 and 10 (Extended Table 1, Fig.3b,c). Since the model predicts relative times, the time-scaling constants A_{NR} and A_{REM} were used to convert values of relative durations to the absolute time units (min).

13. Predictions of NREMS intensity as a function of the initial energy $\varepsilon_{j_{in}}$ and amplitude of x-oscillations. The NREM intensity $I_{NR}(n)$, i.e., the duration of slow-wave sleep (SWS or slow wave activity), is maximal in the first NREMS episode ($n = 1$) and rapidly decreases over consecutive sleep cycles. This behavior correlates positively with the intensity of *x*-oscillations (Fig.3d), presumably because relative intensities of some processes underlying SWS are regulated by *x* and may follow similar oscillatory dynamics. At each level $j = j(n)$ occupied by the wavepacket in the energy relaxation process, we expect that $I_{NR}(n)$ is proportional to the intensity of x-oscillations, i.e., the square of x-amplitudes $L^2(\varepsilon_J)$: $I_{NR}(n) = \kappa(\varepsilon_{j(n)}) * L^2(\varepsilon_{J(n)})$, where the coefficient $\kappa(\varepsilon_{j(n)})$ regulates an efficiency of SWS generation over the entire sleep process. The *k*-coefficient should be maximal at the upper *j* level and decline at lower levels: $\kappa(\varepsilon_j) = const/\ |\varepsilon_j|$. Note that the energies of the bound waves are negative $-1 < \varepsilon_j < 0$ and the absolute value $|\varepsilon_{j(n)}|$ increases as the level index $j(n) = j_{in} + 1 - n$ decreases in the energy relaxation process.

The Morse potential is asymmetric and the measure of the amplitude of non-harmonic <u>*x*</u>-oscillations can be a distance $L(\varepsilon)$ between the right and left classical turning points (Fig. 2a). For the wavepacket bouncing between the walls of the Morse potential, the oscillation amplitude $L(\varepsilon)$ is expressed through the width of the potential well σ and the wavepacket energy ε:

$$L(\varepsilon) = 2\sigma \ln \left[\frac{1+\sqrt{1-|\varepsilon|}}{\sqrt{|\varepsilon|}} \right], \qquad (11)$$

were the value of ε in the *n*-th sleep cycle is given by $\varepsilon_{j(n)}$ in equation 4, with $j = j(n)$. Theoretical values of $I_{NR}(n)$ can be normalized to the first cycle and results are given by the formula:

$$\frac{I_{NR}(n)}{I_{NR}(1)} = \frac{|\varepsilon_{j_{in}}|}{|\varepsilon_{j(n)}|} \left(\frac{L(\varepsilon_{j(n)})}{L(\varepsilon_{j_{in}})} \right)^2, \qquad (12)$$

were the wavepacket energies $\varepsilon_{j(n)}$ and oscillation amplitudes $L(\varepsilon_{j(n)})$ are given by equations 4 and 11 with $j = j(n)$. In Figure 3d, theoretical predictions of relative NREMS intensities for different sleep cycles are compared to experimental data obtained from independent groups of healthy volunteers studied under regular sleep conditions and extended sleep conditions (Method 16, below). It is important to note that the theoretical predictions for $I_{NR}(n)$ in equation 12 do not include any adjustable parameters, and all necessary model parameters were inferred from the observed durations of REMS and NREMS episodes (Extended Table 1, Fig. 3b,c).

14. Dynamics of REMS intensity depends on energy release. According to the model, the rise of REMS intensity $I_R(n)$ with *n* reflects an increase in the portion of energy $\Delta\varepsilon(j(n))$ released within the *n*-th REMS episode, $I_R(n) \propto \Delta\varepsilon(j(n))$. Theoretical values for $I_R(n)$, scaled to REM intensity in the first REMS episode (*n*=1), show linear dependence on the cycle order number *n*:

$$\frac{I_R(n)}{I_R(1)} = \frac{\Delta\varepsilon(\ j_{in} + 1 - n)}{\Delta\varepsilon(j_{in})} = 1 + \frac{n-1}{\sqrt{2}\,\sigma - j_{in}} \qquad (13)$$

Figure 3e illustrates the theoretical linear dependence of REM intensity on *n*, calculated using equation 13 with the values of σ and j_{in} determined in the analysis of REMS and NREMS episode durations for the regular sleep opportunity group (Extended Table 1, Method 16). The slope of the theoretical curve $1/(\sqrt{2}\,\sigma - j_{in})$ depends on two model parameters through the single combination $(\sqrt{2}\,\sigma - j_{in})$ that indicates an approximate number of energy levels above j_{in}. The slope of $I_R(n)/I_R(1)$ increases as the initial level j_{in} approaches the maximal value

$j_{Max} = \left[\sqrt{2}\sigma - \frac{1}{2}\right]$. Our theoretical predictions for relative REM intensities were computed without any fitting parameters and are in excellent agreement with experimental data collected by others[28,33] in two independent groups of young healthy subjects, as shown in Figure 3e.

15. Sleep Cycle Invariant. The wave model predicts the existence of a value that remains constant over consecutive sleep cycles, the Sleep Cycle Invariant (SCI). The SCI is defined as the product of the NREMS episode duration, $T_{j(n)}$, and the REMS episode intensity, $I_R(n)$:

$$T_{j(n)} \ * \ I_R(n) = \frac{2\pi}{\Delta\varepsilon(j(n))} * const * \Delta\varepsilon(j(n)) = 2\pi * const. \quad (14)$$

The SCI value does not depend on the value of energy gap, $\Delta\varepsilon(j)$, and can serve as a signature of sleep cycle integrity or overall sleep quality. Note that, while calculating SCI for the first sleep cycle, the shorter duration of $T_{j(n=1)}$ (due to x_o position; Fig. 2b,c) has to be accounted for and the experimental value for $T_{j(n=1)}$ has to be multiplied by 4/3.

16. Datasets. The model was validated against several sets of polysomnographic data collected under well-controlled conditions of sleep laboratory in groups of young healthy subjects with normal sleep patterns. Those presented in Figure 3 are described below:

(a) *Regular Sleep Opportunity protocol.* The representative group data for regular sleep shown in Figures 1b and 3b,d were part of our larger study on the circadian regulation of sleep and hormonal functions ("Multimodal Circadian Rhythm Evaluation" PI: IVZ), which will be reported in full elsewhere. The study was conducted in accordance with the Declaration of Helsinki on Ethical Principles for Medical Research Involving Human Subjects, adopted by the General Assembly of the World Medical Association, and approved by the Boston University Institutional Review Board. All the participants provided written informed consent. The subjects were 24 young healthy male volunteers (Mean ±SEM: 24.5 ± 4.4 years of age, ranging19-34 years of age) who were selected based on the following self-reported criteria: 7-9 hours of habitual nighttime sleep, small (<1.5h) changes in sleep length on weekends, no sleep complaints, no history of chronic disorders or regular medications, no recent trans-meridian travel, no drug use, no smoking, habitual coffee consumption not exceeding 3 cups a day.

Over the two weeks prior to the inpatient part of the study, the sleep-wake cycle was documented using activity monitors (Phillips Inc.) and a sleep log. Starting on Friday night, subjects spent 3 consecutive nights in the General Clinical Research Center of Boston University School of Medicine. The time in bed was scheduled individually to correspond to the habitual bedtime and subjects were allowed to stay in bed for 9 consecutive hours. Sleep was recorded using polysomnography (Nihon Kohden PSG system), as per standard techniques, and the sleep stages were visually scored for consecutive 30-s epochs[46]. To be included into the regular sleep data set, individual sleep nights had to satisfy the following criteria: sleep efficiency of not less than 85% and the absence of sleep apnea or other symptoms of sleep disorders (n=39 nights total). NREMS-REMS cycles were defined by the succession of a NREMS episode of at least 10 min duration and a REMS episode of at least 3 min duration. No minimum criterion for REMS duration was applied for the completion of the last cycle. A NREMS episode was defined as the time interval between the first two epochs of stage 2 and the first occurrence of REMS within a cycle. A REMS episode was defined as the time interval between two consecutive NREMS episodes or as an interval between the last NREMS episode and the final awakening.

(b) *Extended Sleep Opportunity protocol* is described in detail in the original reports by Barbato & Wehr[30] and Barbato et al.[29], In brief, the study was conducted in 11 healthy male volunteers, 20-34 years of age. The subjects were studied for 4 weeks, with regular activities over 10 hours of light and bedrest over 14 hours of

darkness, when they were encouraged to sleep. The total of 308 sleep records were analyzed. The data used in the present study (Fig. 3c,d) were obtained from Tables 1-3 of [30] and Table 2 of [29], in consultation with Dr. Barbato.

(c) REMS intensity (REM density) data presented in Figure 3e was obtained from the original reports by Aserinsky[28] (11 normal subjects, young males and females) and Marzano et al.[33] (50 normal subjects, young males and females). In both studies, the subjects were identified as university students. The REM density data per sleep cycle of baseline night recordings were obtained from p. 550 of [28] and Figure 1 of [33].

17. Statistical Testing

Goodness of fit was assessed using one-sided χ^2 test, with the degrees of freedom equal to $n - 1 - p$, where n is the number of independent sleep cycle values being fit, and p is the number of model parameters being fit ($p = 4$ for episode duration fits, and $p = 0$ for intensity fits). Note that due to the normalization employed, the number of independent sleep cycle values in each plot is one less than the number of cycles shown. χ^2 and R^2 calculations were carried out using standard R functions.

Bibliography in Methods only:

36. Mott, NF & Massey, HSW, *Theory of Atomic Collisions*, 1965, Oxford, ISBN: 0198512422
37. Migdal, AB, *Qualitative Methods in Quantum Theory*, 2000, CRC Press eBook, 2019 doi.org/10.1201/9780429497940
38. Bates, DR and Lynn, N, Electron Capture of the Accidental Resonance Type, *Proceedings of the Royal Society of London. Series A, Mathematical and Physical Sciences*, Nov. 24, 1959, Vol. **253**, No. 1273, pp. 141-153
39. Goldberger, M.L. and Watson K.M., *Collision Theory*. Dover Publications, Inc., Mineola, N.Y., 2004.
40. Zhu, C. Analytical semiclassical theory for general non-adiabatic transition and tunneling, *Phys. Scr.* **80** (2009) 048114 (9pp), doi: 10.1088/0031-8949/80/04/048114
41. Sun, G, et al., Observation of coherent oscillation in single-passage Landau-Zener transitions. *Sci Rep.* 2015 Feb 16;**5**:8463. doi: 10.1038/srep08463. PMID: 25684697; PMCID: PMC4329555.
42. Tayebirad, G., et al., Time-resolved measurement of Landau-Zener tunneling in different bases, 2010, *Phys.Rev.A*, **82**, 013633, doi: 10.1103/PhysRevA.82.013633
43. Rubbmark, JR, Kash ,MM, Littman, MG, and Kleppner, D, Dynamical effects at avoided level crossings: A study of the Landau-Zener effect using Rydberg atoms, 1981, *Phys.Rev.A*, **23**,3107
44. Cote, R, *Role of Resonances at Ultracold Temperatures*, 2018, pp.313-388 in the book Cold Chemistry: Molecular Scattering and Reactivity Near Absolute Zero (Eds. O. Dulieu and A.Osterwalder), ISBN: 9781782625971
45. Coveney, PV, Child, MS, Barany, A. The two-state S matrix for the Landau-Zener potential curve crossing model: predissociation and resonant scattering, 1985, *Journal of Physics B: Atomic and Molecular Physics* **18** (23), pp.4557-4580 doi:10.1088/0022-3700/18/23/009
46. Berry, RB, et al., AASM Scoring Manual Updates for 2017 (Version 2.4). *J Clin Sleep Med.* 2017 May 15;**13**(5):665-666. doi: 10.5664/jcsm.6576. PMID: 28416048; PMCID: PMC5406946.

Financial support and acknowledgments: This work on mathematical modeling of sleep process was supported by the Chaikin-Wile Foundation (UConn, PI: V.K). Experimental sleep research was supported by Pfizer Inc. (BU, PI: I.V.Z.). We thank Peter Kharchenko for constructive discussions and valuable advice, Olga Kharchenko for illustrations and Walter Lehan for technical assistance in polysomnographic data collection and analysis.

Author contributions: V.K. and I.V.Z. designed research; I.V.Z performed sleep research; V.K. conducted mathematical modeling; V.K., and I.V.Z. wrote the paper. Authors declare no competing interests.

Correspondence and requests for materials should be addressed to vkharchenko@cfa.harvard.edu and irina.zhdanova@bio-chron.com

The dataset generated by the co-author (IVZ) and analyzed during the current study (Method 16, Regular sleep) is available from the corresponding author on reasonable request.
The mathematical algorithms of the wave model of sleep dynamics in "Wolfram Mathematica" format are available from the corresponding author on reasonable request.

Extended data:

Table 1 The Wave Model of Sleep parameters for groups with Regular and Extended sleep.

Group	U_s width σ	Initial level j_{in}	Resonance level j_c	Resonance width Γ
Regular sleep	10	10.3	7.1	0.44
Extended sleep	11.3	11.8	7.6	0.52

Regular sleep: 9-h regular nighttime sleep opportunity, described in Method 16.
Extended sleep: 14-h extended nighttime sleep opportunity, described by Barbato and Wher[30].
At sleep onset, ε can slightly deviate from exact U_s level, hence j_{in} in model approximation appears non-integer. However, at x_o (Fig. 2a) the wavepacket would occupy the closest integer level. Time-scaling constants to convert relative duration values to absolute time (min) and for these groups, A_{NREM} and A_{REM} were, respectively, 0.6 and 23 for Regular sleep and 0.5 and 22 for Extended sleep.

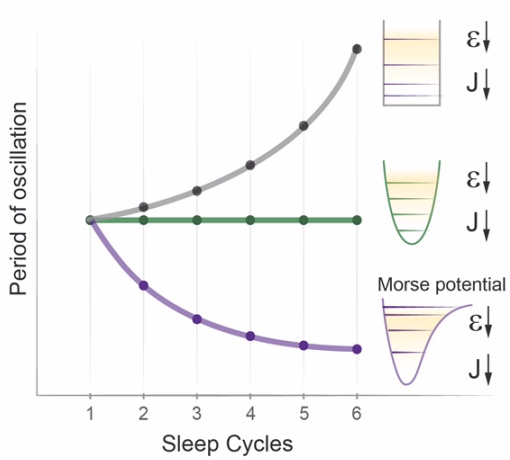

Extended Fig. 1 Consecutive periods of energy relaxation in potential wells of different shape.

The dynamics of energy ε relaxation over consecutive cycles toward the lowest energy level j depends on the shape of the potential well and energy gaps between levels. The period of oscillation is inverse proportional to the energy gap. For rectangular potential (black), top-to-bottom reduction of energy gaps leads to gradual increase in cycle period during energy decline. For a parabolic well (green), equal energy gaps lead to periods of equal duration (harmonic oscillator). For asymmetric Morse potential (purple), gradual top-to-bottom increase in energy gaps leads to a decline in the period of oscillations during energy relaxation.

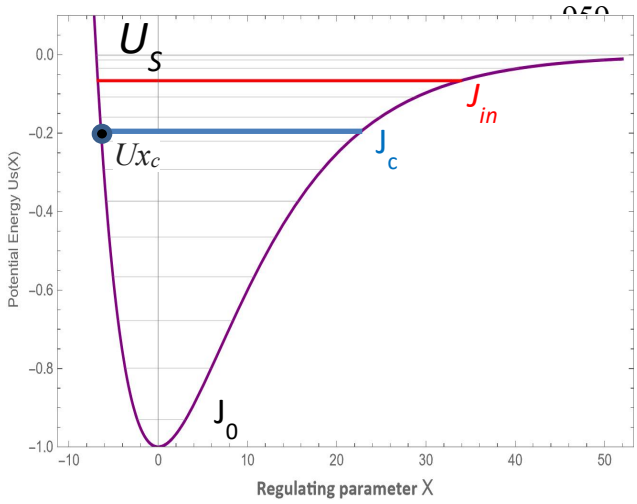

Extended Fig. 2. Actual position of the initial and resonance levels within the *Us* potential well.

For regular sleep (main Fig. 3b, Extended Table 1), typical position of the initial *Us* energy level (J_{in}, red line) of sleep onset is around level 10. The energy of the resonance level (Jc blue line) is around *Us* levels 7, near the homeostatic energy threshold, Ux_c (black dot). Note that Jc does not belong to *Us* and can be positioned asymmetrically relative to *Us* levels (thin horizontal lines). Conventionally, energy levels are counted from the bottom of the potential well (J_0). There is a positive correlation between the total number of *Us* levels and the width of the potential well. In cases of regular sleep, the potential well typically includes around 14 levels.